

This discussion paper is/has been under review for the journal Ocean Science (OS).
Please refer to the corresponding final paper in OS if available.

Multi-scale optimal interpolation: application to DINEOF analysis spiced with a local optimal interpolation

J.-M. Beckers^{1,3}, A. Barth^{1,2}, I. Tomazic¹, and A. Alvera-Azcárate¹

¹GeoHydrodynamics and Environment Research, MARE, University of Liège, Sart-Tilman B5,
4000 Liège, Belgium

²Research Associate, F.R.S.-FNRS, Liège, Belgium

³Honorary Research Associate, F.R.S.-FNRS, Liège, Belgium

Received: 7 March 2014 – Accepted: 11 March 2014 – Published: 18 March 2014

Correspondence to: J.-M. Beckers (jm.beckers@ulg.ac.be)

Published by Copernicus Publications on behalf of the European Geosciences Union.

Multiscale optimal interpolation

J.-M. Beckers et al.

Title Page

Abstract

Introduction

Conclusions

References

Tables

Figures

◀

▶

◀

▶

Back

Close

Full Screen / Esc

Printer-friendly Version

Interactive Discussion



Abstract

We present a method in which the optimal interpolation of multi-scale processes can be untangled into a succession of simpler interpolations. First, we prove how the optimal analysis of a superposition of two processes can be obtained by different mathematical formulations involving iterations and analysis focusing on a single process. From the different mathematical equivalent formulations we then select the most efficient ones by analyzing the behavior of the different possibilities in a simple and well controlled test case. The clear guidelines deduced from this experiment are then applied in a real situation in which we combine large-scale analysis of hourly SEVIRI satellite images using DINEOF with a local optimal interpolation using a Gaussian covariance. It is shown that the optimal combination indeed provides the best reconstruction and can therefore be exploited to extract the maximum amount of useful information from the original data.

1 Introduction

Optimal interpolation (in the following noted OI) is well established (e.g. Gandin, 1965; Delhomme, 1978; Bretherton et al., 1976) and a reference tool when analyzing satellite images. The method has therefore been applied in a large number of scientific studies (e.g. Kawai et al., 2006) and operational setups (e.g. Stark et al., 2007; Donlon et al., 2012; Nardelli et al., 2013). To be optimal, the method requires the correct specification of covariance matrices, most of the time given by parametric functions (e.g. Reynolds and Smith, 1994). Another approach for analyzing a set of satellite images (DINEOF) uses the data to create a truncated Empirical Orthogonal Function (EOF) representation of the data set to fill in missing data (e.g. Beckers and Rixen, 2003; Alvera-Azcárate et al., 2005, 2007). The latter method has been favorably compared to OI and been exploited in a series of applications (e.g. Sheng et al., 2009; Ganzedo et al., 2011; Nikolaidis et al., 2013; Wang and Liu, 2014) including operational setups

OSD

11, 895–941, 2014

Multiscale optimal interpolation

J.-M. Beckers et al.

Title Page

Abstract

Introduction

Conclusions

References

Tables

Figures

◀

▶

◀

▶

Back

Close

Full Screen / Esc

Printer-friendly Version

Interactive Discussion



Multiscale optimal interpolation

J.-M. Beckers et al.

Title Page

Abstract

Introduction

Conclusions

References

Tables

Figures

◀

▶

◀

▶

Back

Close

Full Screen / Esc

Printer-friendly Version

Interactive Discussion



(e.g. Volpe et al., 2012). In some situations it appears however that the truncation of the EOfs series rejects some interesting small-scale features by interpreting them as noise (Sirjacobs et al., 2008). This is due to the fact that under clouds the method is not able to recreate those small-scale features using EOfs only and therefore globally rejects small scales by the EOf truncation. Hence there might remain small-scale information not fully exploited. One natural approach would be to first analyze the large scales with DINEOf and then add an analysis of the residuals using a local optimal interpolation. We will show that this simple approach provides good results but is still suboptimal. The purpose of the present paper is thus to recover additional pieces of information in the reconstruction process by optimally combining the DINEOf approach with a local small-scale optimal interpolation approach. The method we will propose is however more general in the sense that we will show how to deal with a situation in which a combination of processes at different scales needs to be analyzed, possibly using different softwares optimized to analyze a specific process. We will then illustrate the approach in the particular situation with DINEOf analyses for larger scales and OI for smaller scales.

Section 2 will present the theory of optimally combining the analyses of two processes. Then a synthetic example in Sect. 3 will serve as a testbed to provide guidelines in selecting an analysis order among a series of possible options identified. The algorithm is then spelled out for the combination of DINEOf and OI in Sect. 4. Finally the application of the method to real data with a validation exercise will be presented in Sect. 5.

2 Multi-scale optimal interpolation

We will present the method in an optimal interpolation framework and use the following notations and assumptions. Without loss of generality, data are considered anomalies with respect to a reference field and are stored in vector \mathbf{d} . The observations are considered imperfect or including representativity errors, so that the observational error

Multiscale optimal interpolation

J.-M. Beckers et al.

Title Page

Abstract

Introduction

Conclusions

References

Tables

Figures

◀

▶

◀

▶

Back

Close

Full Screen / Esc

Printer-friendly Version

Interactive Discussion



is characterized by covariance matrix \mathbf{R} . The analysis will generally be performed on regular grids, hence in locations not necessarily coinciding with the observation points. The so-called observing operator \mathbf{H} (e.g. Kalnay, 2002) allows to define how to retrieve the analysis values at the observational points from the analysis grid. For filling pixels in satellite images, the application of this matrix to the analysis containing all pixels would simply retrieve the pixels where originally data were present.

The field we try to recover is considered to be created by different independent processes with each process characterized by a specific covariance. On the analysis grid, each process therefore defines a different background covariance matrix. We note these matrices \mathbf{B}_s for a specific process s . Since we are in the presence of different independent processes, each one leading to a different covariance matrix \mathbf{B}_s , the covariance of the total field is $\mathbf{B} = \sum_s \mathbf{B}_s$ and includes the contribution of processes at all scales (e.g. Wackernagel, 2003). In this case, the best analysis $\boldsymbol{\phi}$ of data \mathbf{d} including all scales in the sense of optimal interpolation (e.g. Cushman-Roisin and Beckers, 2011) would be given by $\boldsymbol{\phi} = \bar{\mathbf{K}}\mathbf{d}$ with

$$\bar{\mathbf{K}} = \mathbf{B}\mathbf{H}^T(\mathbf{H}\mathbf{B}\mathbf{H}^T + \mathbf{R})^{-1} = \sum_s \mathbf{B}_s\mathbf{H}^T\left(\sum_i \mathbf{H}\mathbf{B}_i\mathbf{H}^T + \mathbf{R}\right)^{-1} = \sum_s \bar{\mathbf{K}}_s \quad (1)$$

and

$$\bar{\mathbf{K}}_s = \mathbf{B}_s\mathbf{H}^T\left(\sum_i \mathbf{H}\mathbf{B}_i\mathbf{H}^T + \mathbf{R}\right)^{-1}. \quad (2)$$

At this stage we observe that the optimal interpolation demands the inversion of $(\sum_i \mathbf{H}\mathbf{B}_i\mathbf{H}^T + \mathbf{R})$. If this can be achieved for the chosen representation of the different \mathbf{B}_s , then the problem of the multi-scale analysis is solved since the optimal interpolation is provided by Eq. (1).

However, sometimes some of the individual matrices \mathbf{B}_s are not explicitly calculated (for example in spline methods, e.g. Brasseur et al., 1996, or 3DVar-NMC implementations, e.g. Parrish and Derber, 1992; Fisher, 2003) and cannot be added to other

Multiscale optimal interpolation

J.-M. Beckers et al.

Title Page	
Abstract	Introduction
Conclusions	References
Tables	Figures
◀	▶
◀	▶
Back	Close
Full Screen / Esc	
Printer-friendly Version	
Interactive Discussion	

matrices before inversion. In other cases, using a single \mathbf{B}_s can lead to very efficient inversions (for example when reduced rank approaches are possible, e.g. Kaplan et al., 2000; Beckers et al., 2006, or localization is used, e.g. Reynolds and Smith, 1994) while when trying the inversion with the sum of \mathbf{B}_s , one cannot exploit anymore the particular structure of the individual \mathbf{B}_s . In such situations we can therefore only suppose that we have efficient tools to calculate $\mathbf{K}_s \mathbf{x}$, i.e. we are able to apply an analysis tool with a single specific background covariance \mathbf{B}_s to any data array \mathbf{x} . Formally the Kalman gain matrix for the sole process s is¹

$$\mathbf{K}_s = \mathbf{B}_s \mathbf{H}^T (\mathbf{H} \mathbf{B}_s \mathbf{H}^T + \mathbf{R})^{-1}. \tag{3}$$

Hence the problem is to find a way to calculate $\bar{\mathbf{K}}_s \mathbf{x}$ when we can only calculate $\mathbf{K}_s \mathbf{x}$.

Here we present the solution for two processes, but by recursion more scales can be taken into consideration. If we have only two processes, we can provide the optimal analysis for each one of them as $\bar{\mathbf{K}}_1 \mathbf{d}$ and $\bar{\mathbf{K}}_2 \mathbf{d}$, and also the overall optimal interpolation $\bar{\mathbf{K}}_1 \mathbf{d} + \bar{\mathbf{K}}_2 \mathbf{d}$ exploiting the following matrix identities (proof in Appendix A):

$$\bar{\mathbf{K}}_1 = \mathbf{K}_1 - \mathbf{K}_1 \mathbf{H} (\mathbf{I} - \mathbf{K}_2 \mathbf{H} \mathbf{K}_1 \mathbf{H})^{-1} \mathbf{K}_2 (\mathbf{I} - \mathbf{H} \mathbf{K}_1) \tag{4}$$

$$= \mathbf{K}_1 - \mathbf{K}_1 \mathbf{H} \mathbf{K}_2 (\mathbf{I} - \mathbf{H} \mathbf{K}_1 \mathbf{H} \mathbf{K}_2)^{-1} (\mathbf{I} - \mathbf{H} \mathbf{K}_1) \tag{5} \text{ Method P1a}$$

$$= (\mathbf{I} - \mathbf{K}_1 \mathbf{H} \mathbf{K}_2 \mathbf{H})^{-1} \mathbf{K}_1 (\mathbf{I} - \mathbf{H} \mathbf{K}_2) \tag{6}$$

$$= \mathbf{K}_1 (\mathbf{I} - \mathbf{H} \mathbf{K}_2 \mathbf{H} \mathbf{K}_1)^{-1} (\mathbf{I} - \mathbf{H} \mathbf{K}_2) \tag{7} \text{ Method P1b}$$

Similar relationships hold for $\bar{\mathbf{K}}_2$ (as we can just interchange indices 1 and 2). We therefore have now a way to calculate the optimal interpolation exploiting the individual analysis tools \mathbf{K}_1 and \mathbf{K}_2 . All formulations are mathematically equivalent but they have the problem that $(\mathbf{I} - \mathbf{K}_2 \mathbf{H} \mathbf{K}_1 \mathbf{H})^{-1}$ or similar inversions are needed. These are not accessible or lead to an expensive inversion for the same reasons we did not want to

¹Carefully note the absence of $\bar{\mathbf{K}}$ to distinguish it from Eq. (2).



Multiscale optimal interpolation

J.-M. Beckers et al.

Title Page

Abstract

Introduction

Conclusions

References

Tables

Figures

◀

▶

◀

▶

Back

Close

Full Screen / Esc

Printer-friendly Version

Interactive Discussion



invert a matrix involving the sum of \mathbf{B}_s . So it seems we have only displaced the problem. However, the important point to observe is that gains $\mathbf{K}_s\mathbf{H}$ or $\mathbf{H}\mathbf{K}_s$ are “smaller than one”² and the matrix inversion can therefore be implemented by a series expansion: For Ξ “smaller than one” we have the convergent series (e.g. Young, 1981)

$$(1 - \Xi)^{-1} = (1 + \Xi(1 + \Xi(1 + \Xi(\dots)))) \quad (8)$$

When applied to a vector \mathbf{x} , this immediately provides the algorithm to calculate $\mathbf{y} = (1 - \Xi)^{-1}\mathbf{x}$ as follows

```

y ← x
Loop
y ← x +  $\Xi\mathbf{y}$ 
End loop

```

(9)

Algorithm 1 : Approximate matrix inversion

10 which will converge to the desired vector \mathbf{y} . In our case, the calculation of $\Xi\mathbf{y}$ only involves successive analyses using \mathbf{K}_1 and \mathbf{K}_2 , which by hypothesis can be done efficiently. Then of course, if we limit the number of iterations, the four formulations (4)–(7) might lead to different results. In fact, it is easy to show that n iterations used in Eqs. (4) and (5) will yield the same results since

$$15 \quad (1 + \Xi_1 + \Xi_1^2 + \dots + \Xi_1^n)\mathbf{K}_2 = \mathbf{K}_2(1 + \Xi_2 + \Xi_2^2 + \dots + \Xi_2^n) \quad (10)$$

with $\Xi_1 = \mathbf{K}_2\mathbf{H}\mathbf{K}_1\mathbf{H}$ and $\Xi_2 = \mathbf{H}\mathbf{K}_1\mathbf{H}\mathbf{K}_2$. Similarly, iterative versions of Eqs. (6) and (7) will also lead to the same analysis. The only difference is possible in terms of computational

²A formal definition of “smaller than one” for the matrices demands the module of their eigenvalues being all smaller than one; see Daley (1993) page 127 for a prove that $\mathbf{H}\mathbf{K}$, which is also sometimes called the hat matrix or influence matrix has eigenvalues between zero and one.

Multiscale optimal interpolation

J.-M. Beckers et al.

Title Page

Abstract

Introduction

Conclusions

References

Tables

Figures

◀

▶

◀

▶

Back

Close

Full Screen / Esc

Printer-friendly Version

Interactive Discussion



load. Since generally the number of observations is much smaller than the number of points on the output grid of the analysis, using Eqs. (5) and (7) during iterations will work on smaller files/arrays and also could benefit from quicker analysis if the analysis tool is faster when asked to output values only at data locations. Hence Eqs. (5) and (7) are two formulations which we will retain and which will differ if iterations on the inversion of $(\mathbf{I} - \mathbf{H}\mathbf{K}_1\mathbf{H}\mathbf{K}_2)$ or $(\mathbf{I} - \mathbf{H}\mathbf{K}_2\mathbf{H}\mathbf{K}_1)$ are not pursued until convergence. For $\bar{\mathbf{K}}_2$ we now write out the two equivalent relevant versions:

$$\bar{\mathbf{K}}_2 = \mathbf{K}_2 - \mathbf{K}_2\mathbf{H}\mathbf{K}_1(\mathbf{I} - \mathbf{H}\mathbf{K}_2\mathbf{H}\mathbf{K}_1)^{-1}(\mathbf{I} - \mathbf{H}\mathbf{K}_2) \quad \text{Method P2a} \quad (11)$$

$$= \mathbf{K}_2(\mathbf{I} - \mathbf{H}\mathbf{K}_1\mathbf{H}\mathbf{K}_2)^{-1}(\mathbf{I} - \mathbf{H}\mathbf{K}_1) \quad \text{Method P2b} \quad (12)$$

The cost for calculating an analysis with $\bar{\mathbf{K}}_1$ or $\bar{\mathbf{K}}_2$ using n iterations is $3 + 2n$ analyses using \mathbf{K}_1 and \mathbf{K}_2 in Eqs. (5) or (11) whereas the use of Eqs. (7) or (12) demands $2 + 2n$ standard analyses. In the following P1a and P2a will refer respectively to the application of Eqs. (5) and (11) with iterations, and P1b and P2b refer respectively to the use of Eqs. (7) or (12).

We also note that even when using iterated versions, using Eqs. (5) and (12) leads to

$$\bar{\mathbf{K}}_1 = \mathbf{K}_1(\mathbf{I} - \mathbf{H}\bar{\mathbf{K}}_2) \quad (13)$$

which will be exploited in our final algorithm.

$\bar{\mathbf{K}}_1$ and $\bar{\mathbf{K}}_2$ allow us to calculate the best analysis for each of the processes. A natural but suboptimal estimate for each process would of course be obtained when using \mathbf{K}_1 for process 1 and \mathbf{K}_2 and for process 2. A slightly more elaborated idea would rather be to use $\mathbf{K}_1(\mathbf{I} - \mathbf{H}\bar{\mathbf{K}}_2)$ and $\mathbf{K}_2(\mathbf{I} - \mathbf{H}\bar{\mathbf{K}}_1)$ so as to get the analysis of one process only using data from which we tried to subtract the information from the other process. Therefore we can also design several simple ways to sub-optimally estimate the overall analysis

using the following gain matrices

$$\tilde{\mathbf{K}}_{00} = \mathbf{K}_1 + \mathbf{K}_2 \quad (14)$$

$$\tilde{\mathbf{K}}_{01} = \mathbf{K}_1 + \mathbf{K}_2(\mathbf{I} - \mathbf{H}\mathbf{K}_1) \quad (15)$$

$$\tilde{\mathbf{K}}_{10} = \mathbf{K}_1(\mathbf{I} - \mathbf{H}\mathbf{K}_2) + \mathbf{K}_2 \quad (16)$$

$$5 \quad \tilde{\mathbf{K}}_{11} = \mathbf{K}_1(\mathbf{I} - \mathbf{H}\mathbf{K}_2) + \mathbf{K}_2(\mathbf{I} - \mathbf{H}\mathbf{K}_1) \quad (17)$$

These simple versions can also be compared later to the iterated versions.

2.1 Error fields

10 The analysis error covariance matrix \mathbf{P}^a when using any gain matrix \mathbf{K} is given by (e.g. Cushman-Roisin and Beckers, 2011)

$$\mathbf{P}^a = \mathbf{B} - \mathbf{B}\mathbf{H}^T\mathbf{Z}^{-1}\mathbf{H}\mathbf{B} + (\mathbf{B}\mathbf{H}^T - \mathbf{K}\mathbf{Z})\mathbf{Z}^{-1}(\mathbf{H}\mathbf{B} - \mathbf{Z}\mathbf{K}^T) \quad (18)$$

$$\mathbf{Z} = (\mathbf{H}\mathbf{B}\mathbf{H}^T + \mathbf{R}) \quad (19)$$

15 When the gain is optimal, the last term vanishes and we get the minimal error of the optimal interpolation approach. Hence we can also assess the errors of the different analyses we propose.

For example, if we are interested in the analysis of process 1 and use the exact form of $\tilde{\mathbf{K}}_1$, the expected error covariance on the analysis of process 1 reads

$$20 \quad \mathbf{P}_1^a = \mathbf{B}_1 - \tilde{\mathbf{K}}_1\mathbf{H}\mathbf{B}_1. \quad (20)$$

Similarly, the error of the analysis of process 2 alone when using the exact form of $\tilde{\mathbf{K}}_2$ reads

$$\mathbf{P}_2^a = \mathbf{B}_2 - \tilde{\mathbf{K}}_2\mathbf{H}\mathbf{B}_2. \quad (21)$$

Title Page	
Abstract	Introduction
Conclusions	References
Tables	Figures
◀	▶
◀	▶
Back	Close
Full Screen / Esc	
Printer-friendly Version	
Interactive Discussion	



Multiscale optimal interpolation

J.-M. Beckers et al.

Title Page

Abstract

Introduction

Conclusions

References

Tables

Figures

◀

▶

◀

▶

Back

Close

Full Screen / Esc

Printer-friendly Version

Interactive Discussion



Case 1: In a first case, we use two processes with unit signal-to-noise ratios but very different correlation length. For process 1 a length scale of 33 grid points was taken whereas for process 2 a length scale of 4.5 grid points was used. The data cover the original grid entirely and the analysis is therefore only checking the filtering properties of the different formulations. Hence we will only look at average behaviors, but distinguish errors in reconstructing process 1, process 2 and the overall field, as detailed in Tables 1–4. For process 1 (Table 1), we note that it is not beneficial to try to subtract the small scale information before the analysis by a simple residual approach (column 3) and that the iterative version P1a even without iterations yields the best results. When performing iterations, Table 1 shows convergence and the superiority of P1a. For small scale process 2 (Table 2), the simple version of first subtracting the large scale analysis from the data performs best and is equivalent to a non-iterated version of P2b. All iterative versions converge and iterative version P2b shows its superiority for small scales.

For the overall analysis, the simple approaches in Table 3 exhibit interesting facts. The best approach is to combine the analysis of one process with the analysis of the residual for the other process. Furthermore, even if we showed that process 1 is best captured by \mathbf{K}_1 and process 2 by analyzing residuals via $\mathbf{K}_2(\mathbf{I} - \mathbf{H}\mathbf{K}_1)$, the overall analysis performs as well when doing the inverse and add the results up. For the iterated version (Table 4), we see a similar pattern, adding up formulations of the same type (P1a + P2a or P1b + P2b) do not perform as well as adding up formulations of different type (P1a + P2b or P1b + P2a), but convergence is observed in all cases. The natural choice for this case is therefore clearly P1a for the larger scales, equation P2b for the shorter scales and their sum for the overall analysis.

For *case 2*, we use the same parameters but look to the behavior when the scales are less well separated and use a correlation length of 16 grid points instead of 4.5 for process 2. Compared to case 1, conclusions remain mostly unchanged, but we observe that more iterations are needed to reach the same quality in the iterated version.

Multiscale optimal interpolation

J.-M. Beckers et al.

Title Page

Abstract

Introduction

Conclusions

References

Tables

Figures

◀

▶

◀

▶

Back

Close

Full Screen / Esc

Printer-friendly Version

Interactive Discussion



For *case 3* and the following, we only use observations in parts of the domain. In one region sampling is done with grid resolution and in other regions with larger parts void of data (up to 20 grid points). This mimics the situation we will encounter with satellite images. Otherwise the case is identical to case 1³. Conclusions for case 3 are similar to case 1 and we see that even with few iterations we capture the maximum information from the data available.

In *case 4* we take the same parameters as in case 3 (partial observation, very different scales), but assume that process 1 has a much higher signal-to-noise ratio: we use a value of 20 instead of 1. In this case, P1a provides again the best analysis for process 1 and P2b for process 2 alone. For the simple approaches for the total field (Table 3), now the selection of the field used to create residuals is important, and as one might have guessed, one has first to analyze the large-scale process with the high signal-to-noise ratio and then add the small-scale analysis of the residuals (it means $\tilde{\mathbf{K}}_{01}$ is used for the global analysis). For the iterated version it is now clearly the combination P1a and P2b which outperforms the others.

Since this case is also similar to our original question, we can now also have a look at the error distribution of the 100 000 realizations (Figs. 1 and 2). They confirm that when the average error of the formulations is close to the error of the truly optimal solution, also the histogram of errors almost coincide, providing evidence that we are indeed very close to the optimal interpolation.

To complete the analysis, some additional cases have been looked at:

In *case 5* we use the same parameters as in case 4 but use the short correlation length for process 1 and the larger one for process 2. Despite this inversion, the same conclusions as in case 4 remain. This means that it is the process with the highest

³Note that when comparing the results of case 1 and case 3, the error has been scaled by the best analysis possible with the data available. Hence a better score in case 3 does not mean the analysis itself is better than the analysis in case 1 (which uses more data) but that we are closer to the best we can get from the data.

optimal interpolation will result. Alternatively if scales are very similar, a single analysis with average correlation length could be used.

4 DINEOF + OI

We now come to the application of our ideas to the better reconstruction of satellite images. DINEOF has proven to be efficient, particularly when looking at larger scales since the interpolation exploits dominant large-scale EOF structures to reconstruct missing data under clouds. Those EOF generally capture a very high percentage of the data variance and in this sense we can assume that the signal-to-noise ratio is high.

If we try to add a local covariance structure with an optimal interpolation approach, the signal-to-noise ratio for this additional process we want to extract is probably much lower. Hence we are in the situation similar to the synthetic case 3 and 4 of the previous section and the iterative version of P1a + P2b is the natural choice, where \mathbf{K}_1 stands for the DINEOF-based analysis and \mathbf{K}_2 for the local OI application. The analyzed field ϕ can be easily obtained from P1a + P2b, called hereafter DINEOFI, programmed as

Multiscale optimal interpolation

J.-M. Beckers et al.

Title Page

Abstract

Introduction

Conclusions

References

Tables

Figures

◀

▶

◀

▶

Back

Close

Full Screen / Esc

Printer-friendly Version

Interactive Discussion



Multiscale optimal interpolation

J.-M. Beckers et al.

Title Page

Abstract

Introduction

Conclusions

References

Tables

Figures

◀

▶

◀

▶

Back

Close

Full Screen / Esc

Printer-friendly Version

Interactive Discussion



$$\phi \leftarrow \mathbf{K}_1 d$$

$$\mathbf{w}_1 \leftarrow \mathbf{H}\phi \text{ (Use only analysis at data points without clouds)}$$

$$\mathbf{w}_1 \leftarrow (d - \mathbf{w}_1) \text{ (Residuals)}$$

Calibrate or check OI parameters at this point using \mathbf{w}_1

$$\mathbf{w}_2 \leftarrow \mathbf{w}_1 \text{ (Start of iterative matrix inversion)}$$

Loop n times

$$\mathbf{w}_2 \leftarrow \mathbf{H}\mathbf{K}_2 \mathbf{w}_2 \text{ (apply tool 2 and retrieve solution at data points)}$$

$$\mathbf{w}_2 \leftarrow \mathbf{H}\mathbf{K}_1 \mathbf{w}_2 \text{ (apply tool 1 and retrieve solution at data points)}$$

$$\mathbf{w}_2 \leftarrow \mathbf{w}_1 + \mathbf{w}_2$$

End loop

$$\omega_1 \leftarrow \mathbf{K}_2 \mathbf{w}_2$$

ω_1 now contains scale 2 field $\bar{\mathbf{K}}_2 d$; can be saved for other uses

$$\phi \leftarrow \phi + \omega_1 \text{ (Add it to } \mathbf{K}_1 d \text{)}$$

$$\mathbf{w}_1 \leftarrow \mathbf{H}\omega_1$$

$$\omega_1 \leftarrow \mathbf{K}_1 \mathbf{w}_1 \text{ (Calculates } \mathbf{K}_1 \mathbf{H}\bar{\mathbf{K}}_2 d \text{)}$$

$$\phi \leftarrow \phi - \omega_1 \text{ (Final analysis)}$$

If scale 1 solution is requested, subtract saved scale 2 solution from ϕ and save it

Algorithm 2: combination of two analysis tools for an optimal interpolation

which shows that the simple application of existing analysis tools to data arrays and a few working arrays/files ($\mathbf{w}_1, \mathbf{w}_2, \omega_1$) will solve our problem and provide the analysis ϕ . This demands $2 + n$ applications of \mathbf{K}_1 and $1 + n$ applications of \mathbf{K}_2 .

5 For the calibration of OI parameters it is probably safe to work on residuals after step 3 (available in intermediate results \mathbf{w}_1) for fitting or verification of the correlation length and signal-to-noise ratio since we showed earlier that if scale separation is good, $\mathbf{K}_2(\mathbf{I} - \mathbf{H}\mathbf{K}_1)d$ is a good proxy of the analysis for process 2.

10 There remains to formulate how \mathbf{K}_1 and \mathbf{K}_2 are defined. If during step 1 of the algorithm ϕ could be interpreted as the DINEOF result (and hence \mathbf{K}_1 the DINEOF tool applied to the data), in the subsequent part of the algorithm we cannot just replace

Multiscale optimal interpolation

J.-M. Beckers et al.

Title Page

Abstract

Introduction

Conclusions

References

Tables

Figures

◀

▶

◀

▶

Back

Close

Full Screen / Esc

Printer-friendly Version

Interactive Discussion



\mathbf{K}_1 by “apply DINEOF”, since the EOFs calculated are data dependent. Hence when working with residuals in the later steps, we would not use the same covariances as in the first step. So instead of “applying DINEOF”, we can use the EOFs calculated by DINEOF on the raw data to specify covariance matrices as in Beckers et al. (2006).

5 For such an optimal interpolation using EOFs from DINEOF, we recall that DINEOF provides the Singular Value Decomposition (SVD) of the data⁴ stored in a $m \times n$ matrix \mathbf{X} with m pixels for each cloud-free image and n images as

$$\mathbf{X} = \mathbf{U}\mathbf{\Sigma}\mathbf{V}^T \quad (23)$$

10 The N spatial EOFs (stored in the $m \times N$ matrix \mathbf{U}) and temporal EOFs (stored in the $n \times N$ matrix \mathbf{V}) can be used together with the singular values (stored in the diagonal matrix $\mathbf{\Sigma}$) to estimate the spatial covariances so that we can spatially interpolate/analyze each of the n images exploiting covariance matrix

$$\mathbf{B}^{(s)} = \frac{1}{n} \mathbf{U}\mathbf{\Sigma}^2\mathbf{U}^T \quad (24)$$

15 For a spatial analysis of image j , the gain matrix reads

$$\mathbf{K}^{(s)j} = \mathbf{B}^{(s)}\mathbf{H}^T (\mathbf{H}\mathbf{B}^{(s)}\mathbf{H}^T + \mathbf{R})^{-1}. \quad (25)$$

20 Note that for each image j , another observation operator \mathbf{H} is used as the cloud coverage changes. In order not to overload notations we do not add an index but remember that \mathbf{H} is image dependent.

The computational efficiency of this method stems from the fact that the application of the Woodbury matrix identity (e.g. Golub and Van Loan, 2012) translates this into a least square fitting of N modes (e.g. Beckers et al., 2006). Assuming independent and identical observational errors of variance e^2 , this leads to

$$\mathbf{K}^{(s)j} = \mathbf{L} \left(e^2 \mathbf{I} + \mathbf{L}_p^T \mathbf{L}_p \right)^{-1} \mathbf{L}_p^T \quad (26)$$

⁴We stress again that averages have been subtracted to work with anomalies.

with $\mathbf{L} = \mathbf{U}\boldsymbol{\Sigma}/\sqrt{n}$ and the corresponding version for the data present in each image $\mathbf{L}_p = \mathbf{H}\mathbf{L}$ (note that here \mathbf{H} still changes for each image). The computational efficiency is now understood as for each image the matrix to invert is of size $N \times N$ when using Eq. (26) instead of $p \times p$ when using Eq. (25), with the number N of retained EOFs much smaller than the number p of pixels in an image.

By symmetry we can also choose to perform a temporal interpolation of each of the m pixels by using for pixel i the time interpolation from covariance

$$\mathbf{B}^{(t)} = \frac{1}{m} \mathbf{V}\boldsymbol{\Sigma}^2 \mathbf{V}^T \quad (27)$$

and use the computationally efficiently calculated gain matrix

$$\mathbf{K}^{(t)i} = \mathbf{T} \left(\epsilon^2 \mathbf{I} + \mathbf{T}_p^T \mathbf{T}_p \right)^{-1} \mathbf{T}_p^T \quad (28)$$

with $\mathbf{T} = \mathbf{V}\boldsymbol{\Sigma}/\sqrt{m}$ and $\mathbf{T}_p = \mathbf{H}\mathbf{T}$ (here \mathbf{H} changes for each of the pixels and selects the images in which the pixel is not clouded).

So we can choose to spatially interpolate each image to get an overall analysis or to temporally interpolate each pixel to get the overall analysis. Instead of choosing one or the other method we can again apply the basic idea of the present paper allowing to combine two analysis tools. We can indeed use as a covariance the combination of the spatial and temporal covariances and for a pixel i of image j the covariance with a pixel i' of image j' is modeled as $\mathbf{B}_{ij'}^{(s)} \delta_{jj'} + \mathbf{B}_{ij'}^{(t)} \delta_{ii'}$ with the standard Kronecker⁵ symbol $\delta_{ij'}$. In other words, as we are in the presence of the combination of two covariances, without actually creating the sum and full gain matrix, we can use again the iterated versions P1a + P2b where process 1 is now provided by the spatial interpolation tool and process 2 by the temporal interpolation tool. This “inner” iterative combination provides then our EOF based analysis tool \mathbf{K}_1 for the “outer” combination method with a local OI.

⁵ $\delta_{ij'}$ is one when $i = i'$, zero otherwise.

Multiscale optimal interpolation

J.-M. Beckers et al.

Title Page

Abstract

Introduction

Conclusions

References

Tables

Figures

◀

▶

◀

▶

Back

Close

Full Screen / Esc

Printer-friendly Version

Interactive Discussion



So if it is clear that in the later steps of our Algorithm 2 we use \mathbf{K}_1 as just described (the combination of spatial and temporal EOF-based covariances), the first step could still be taken as the DINEOF analysis as it could be regarded as some kind of best first guess. This option will be looked at later.

For \mathbf{K}_2 , a standard optimal interpolation tool is used. In practice, the OI application for satellite images repeated at the same locations can be strongly optimized since it is easy to collect the data points which are within reach of the covariance function at any given point in which the analysis is demanded. As the correlation length will be small, the number of data points involved will be small also and the matrix inversion very quick for each analysis point. The typical parametric correlation function c used in optimal interpolation is a Gaussian

$$c = e^{-\left(\frac{\delta x}{L_x}\right)^2} e^{-\left(\frac{\delta y}{L_y}\right)^2} e^{-\left(\frac{\delta t}{T}\right)^2} \quad (29)$$

where δx , δy and δt are the difference in space and time coordinates between the two points for which we want to calculate the covariance. L_x and L_y are then the correlation length-scale in x and y direction and T the correlation timescale. The correlation function has to be multiplied by variance σ_2^2 to provide \mathbf{B}_2 . For the implementation of this optimal interpolation we used the open-source code `optiminterp` available at <http://octave.sourceforge.net/optiminterp/overview.html>⁶. Its use was computationally optimized by exploiting the fact that for each point in which the analysis is demanded the gridded nature of the data points allows a direct selection of possibly involved data points and a rejection of all others. So in means one can feed the analysis only with data in a box of size $4L_x \times 4L_y \times 4T$ centered around the analysis point, which greatly reduces sorting and selecting time and also allows for a parallel execution.

⁶Or http://modb.oce.ulg.ac.be/mediawiki/index.php/Optimal_interpolation_Fortran_module_with_Octave_interface

Multiscale optimal interpolation

J.-M. Beckers et al.

Title Page	
Abstract	Introduction
Conclusions	References
Tables	Figures
◀	▶
◀	▶
Back	Close
Full Screen / Esc	
Printer-friendly Version	
Interactive Discussion	



5 Test case

For the real case application, we use an interesting SST hourly dataset derived from Spinning Enhanced Visible and Infrared Imager (SEVIRI) onboard Meteosat Second Generation (MSG) geostationary satellite and produced operationally by the European Organisation for the Exploitation of Meteorological Satellites (EUMETSAT) Ocean and Sea Ice Satellite Application Facility (OSI-SAF) at Meteo-France/Centre de Meteorologie Spatial (CMS) in Lannion (EUMETSAT, 2011; Le Borgne et al., 2011). Because of its geostationarity, high-frequency sampling is available and analyses resolving the daily cycle appeared (e.g. Marullo et al., 2010, 2013). Some high frequency content is expected to be filtered by standard DINEOF applications and therefore the data should provide a good testbed for our new method. Furthermore, capturing the diurnal cycle in using satellite-derived sea surface temperature is considered an important challenge (Stuart-Menteth et al., 2003) and several studies have been performed recently using hourly data (Karagali et al., 2012; Le Borgne et al., 2012; Eastwood et al., 2011).

Excellent results when using SEVIRI data have been obtained (Marullo et al., 2013): by combining a dynamical model resolving the daily cycle with the SEVIRI data, their reconstruction of hourly data covering the whole Mediterranean Sea during the three month summer period of 2011 showed rms (root mean square) errors compared to in-situ data of 0.64K with off-shore moorings and 0.47K with drifter data, with a well resolved daily cycle. A synthetic cloud cross validation exercise also provided a rms difference of only 0.16K between the artificially clouded SEVIRI points and their reconstruction. In their case the artificial clouds were constructed by moving a 200 km wide meridional band of “clouds” westward across the domain in around 24 h, so that no persistent artificial clouds were included.

For our study focusing on the methodology rather the reconstruction itself, we selected a smaller data set, covering the period of 1–16 August 2013. This data set has some clear images with daily cycles on which artificial clouds can be added for validation purposes. The spatial resolution of the data is 0.05° , available at hourly frequency,

Title Page

Abstract

Introduction

Conclusions

References

Tables

Figures

◀

▶

◀

▶

Back

Close

Full Screen / Esc

Printer-friendly Version

Interactive Discussion



leading to $n = 16 \times 24 = 384$ images. In all cases we used all data with quality flags 4 or 5 (acceptable and best quality). In order to assess the robustness of the method and the conclusions of this experiment we look at four different cases.

Two different spatial coverages were considered, one looking only at the Western Mediterranean Sea, the other to the whole Mediterranean Sea. This approach allows to check the robustness of the statistical results and the effect of different EOF structures, and also shows the effect of a larger data variability. For the Western Mediterranean Sea we retrieve images of $327 \times 217 = 70\,959$ pixels from which 29 380 fall on land, so that the maximum number of pixels in each image useful for analyses is $m = 41\,579$. Without additional artificial clouds this data set presents an average cloud coverage of 29.70%. For the whole Mediterranean Sea, images have 850×320 pixels, from which 120 343 fall onto the sea so that $m = 151\,566$ (see Fig. 3). The average cloud coverage is 23.53% in this case. We also note that for the setup over the whole Mediterranean Sea, data from the Black Sea and the Atlantic Sea are included, making the test more challenging as the EOF structures will need to cope with different, mostly unconnected, variabilities.

For cross validation purposes, additional clouds will be added to the original data. The so clouded cross-validation data are never used in the calculations (neither in the DINEOF decomposition nor the different optimal interpolations) but allow the computation of metrics characterizing the quality of the analysis under clouds. The rms error δ_D of the DINEOF reconstruction under these additional clouds can be used as a reference error which we want to improve. We can then define a skill-score S as

$$S = 1 - \frac{\delta^2}{\delta_D^2} \quad (30)$$

which measures the relative increase in precision (a zero skill-score value indicates no better results than DINEOF whereas a value of 1 means a perfect reconstruction). A second standard metric for the validation is the correlation coefficient between the analysis and the cross-validation points noted r .

Multiscale optimal interpolation

J.-M. Beckers et al.

Title Page

Abstract

Introduction

Conclusions

References

Tables

Figures

◀

▶

◀

▶

Back

Close

Full Screen / Esc

Printer-friendly Version

Interactive Discussion



Multiscale optimal interpolation

J.-M. Beckers et al.

Title Page

Abstract

Introduction

Conclusions

References

Tables

Figures

◀

▶

◀

▶

Back

Close

Full Screen / Esc

Printer-friendly Version

Interactive Discussion



Two different kinds of artificial cloud sets allow to check the effect of more or less persistent cloud coverage on the reconstruction quality and the improvements brought by our new method. In one situation, clouds from the last two weeks of July 2013 are superimposed to the already present clouds and the pixels masked in this way taken aside as cross-validation data. In the other situation we generate artificial clouds as in Marullo et al. (2013): the slab of clouds moves from east to west across the domain in about one day and then starts again from the east. The fraction of overlap between successive images was taken similar to the one in Marullo et al. (2013).

From these two different spatial coverages and two different cloud coverages we create our four test cases:

Setup 1: Western Mediterranean Sea, added July clouds

For cross validation purposes, clouds from the last two weeks of July were superimposed, resulting in total average cloud coverage which increases from 29.70% to 42.06%. The data set is then analyzed with DINEOF, providing $N = 38$ EOFs, the singular values and the DINEOF reconstruction explaining 91% of the variance. As expected DINEOF, captures a large part of the variability. A first diagnostic can be performed by calculating the root mean square difference between this reconstruction and the artificially clouded pixels (the cross-validation points, here we have 1973 438 of them) and we obtain an associated standard deviation $\delta_D = 0.496$ K close to the noise level in the data, as the SEVIRI SST standard deviation is around 0.5 K (Brisson et al., 2002). For DINEOF we obtain $r = 0.9371$, which is therefore the baseline to improve in this case.

For this case and the following, the metrics of the standard DINEOF application just mentioned are summarized in Table 5 and for the following cases we only describe the cross-validation approach.

Multiscale optimal interpolation

J.-M. Beckers et al.

Title Page

Abstract

Introduction

Conclusions

References

Tables

Figures

◀

▶

◀

▶

Back

Close

Full Screen / Esc

Printer-friendly Version

Interactive Discussion



Setup 2: Western Mediterranean Sea, added banded clouds

In the first setup, analyses under persistent large scale clouds can of course not be improved by the local optimal interpolation. To check if we can reconstruct data under fast moving clouds, we take a band of westward moving “clouds”.

Setup 3: Whole Mediterranean Sea, added July clouds

To check how the reconstructions behave when a larger range of observations are present, we look at the whole Mediterranean Sea. The full Mediterranean Sea case exhibits generally less clouds (23.53%) and with the July clouds added to the original data the cloud coverage increases to 35.29%.

Setup 4: Whole Mediterranean Sea, added banded clouds

Finally we complete the comparisons by using the whole Mediterranean Sea, but with a fast moving westward band of “clouds”.

To proceed, we now need to specify the observational error variance and the variance σ_2^2 for the local optimal interpolation in each case. As we will show later, the conclusions remain robust in all cases and we will only detail results of the most challenging Setup 3. The parameter optimization of the other cases was performed in a similar way with similar results.

To specify the covariance function to be used with the local optimal interpolation, we can take advantage of two particularities of the data we will analyze: we expect them to contain mainly small scales (as we work on residuals) and we have a rather large amount of data available on a regular grid to fit the parametric covariance function. The following approach exploits these two particularities.

For the longitude correlation length, we can randomly select a point in the dataset and verify if a prescribed number of consecutive data is present in the longitudinal

Multiscale optimal interpolation

J.-M. Beckers et al.

Title Page

Abstract

Introduction

Conclusions

References

Tables

Figures

◀

▶

◀

▶

Back

Close

Full Screen / Esc

Printer-friendly Version

Interactive Discussion



direction. Since we are looking at small scales, typically 20–50 points of consecutive data would be enough to capture signals and the probability to find such a chunk of complete data is high enough. Once found such a chunk, we can apply a Fast Fourier Transform to it and calculate the squared Fourier amplitude. This is repeated a large number of times (10 000 in our case) and an average squared amplitude spectrum can be assessed. The autocovariance function can then be calculated as the inverse Fourier transform of this square of the amplitude spectrum of the signal (e.g. Bracewell, 1986). This autocovariance from the data can then finally be used to fit the analytical function and estimate the signal-to-noise ratio. In practice, the fitting is done by trying to fit the Gaussian function $\alpha \exp(-\beta \delta_x^2)$ to the points of the data-based autocorrelation function up to the zero-crossing but eliminating the zero-lag point. The signal-to-noise ratio can finally be estimated by (see Fig. 4)

$$\lambda_2 = \frac{\alpha}{1 - \alpha} \quad (31)$$

where α is the fitted value representing the signal and $1 - \alpha$ the part not explained by the correlation function, hence the noise.

The same approach is then also applied to latitude and time, and since the fitting is not perfect, the estimated overall signal-to-noise ratio is conservatively taken as the lowest one found from the three directions.

We note on Fig. 4 that the time autocorrelation spectrum exhibits an anti-correlation at 6 h and maximum autocorrelation at 12 h. This reflects in fact the asymmetry of the diurnal cycle. When analyzing the raw data instead of residuals, the spectrum and autocorrelation (not reproduced here) indeed shows an anti-correlation at 12 h and correlation at 24 h. Thus the residuals will allow to follow the higher frequency content.

The observational noise variance was fixed as $0.25K^2$. A sensitivity analysis was performed, changing this value in the range of $0.1K^2$ to $10K^2$. In all cases, the conclusion in terms of ranking of the different methods remained the same, only the relative part of the solution picked up by the EOF-based covariances or local optimal interpolation was affected. As the value of $0.25K^2$ is the typical value associated with SEVIRI

tendency of DINEOF reconstructions dampening the extreme variations is reduced with the new method).

Since the computational load of the new method is a fraction of the computational cost of the DINEOF decomposition (typically 10% for the iterated version) it is the natural choice to improve DINEOF results when good skill scores and correlations are sought. If one does not want to program \mathbf{K}_1 and iterations⁷, the simple approach of using DINEOF followed by the local optimal interpolation of residuals is a simple alternative.

Skill scores and correlation coefficients are not the only criteria to select a method and we can further check if the new method also leads to better feature reconstruction.

Figure 7 shows the analysis, residuals and the y-autocorrelation for the standard DINEOF approach and our new iterated solution DINEOFOI. While DINEOF residuals exhibit patterns identified in the autocorrelation function, the residuals of the new method are almost pure spatially uncorrelated noise. For the other methods, not shown here, \mathbf{K}_1 and DINEOF+iterations both contain a similarly autocorrelated signal as DINEOF. All other methods are able to retrieve this structure and leave mostly spatially uncorrelated residuals. We also see that the amplitude of the daily cycle is now closely following the data (Fig. 3).

Looking into the North Western Mediterranean Sea (Fig. 8), the typical lower temperature structures are also used in model validations (e.g. Millot, 1987; Beckers et al., 2002). Here the comparison of the reconstructions with the cross-validation data not used also reveals that some features are now better visible in the reconstruction with the new method, in particular the form of the cold patch in the center of the domain.

Instead of looking at the full analysis, we can also focus on individual processes 1 and 2. For example, the time evolution at latitude 34.375°N in the Eastern Mediterranean Sea (Fig. 9) shows clearly how scale 1 solution is dominated by the daily cycle (we even see the earlier heating in the eastern part during the day). Scale 2 on the

⁷To avoid reprogramming \mathbf{K}_1 and iterations, the code will be made available at <http://modb.oce.ulg.ac.be/mediawiki/index.php/DINEOF>

Multiscale optimal interpolation

J.-M. Beckers et al.

Title Page

Abstract

Introduction

Conclusions

References

Tables

Figures

◀

▶

◀

▶

Back

Close

Full Screen / Esc

Printer-friendly Version

Interactive Discussion



other hand has a 12 h period component and whose structure could lead to interesting interpretations.

Satellite images are also often used to track features and fronts. To do so, Sobel edge detector methods are typically applied (e.g. Simpson, 1990). If we do so, even when first applying a median filter, raw data do not allow front detection (upper left panel of Fig. 10). With DINEOF we clearly see, among others, structures related to the Algerian current instability (e.g. Millot, 1987; Beckers and Nihoul, 1992). With our new method, the overall analysis includes short scale signals and therefore gradient detectors are slightly more noisy. However if we look at results for scale 1 process alone (upper right panel) we recover more robust results. Hence for front detection DINEOF remains a natural choice as it dampens out higher frequency signals and shows that DINEOF effectively resolves the larger scales. Only if smaller scales are important, adding the local optimal interpolation (either in simple or iterated version) is recommended, but one must be aware that in regions with large scale persistent clouds no improvement over DINEOF can be expected.

6 Conclusions

We presented a general framework for multi-scale analysis using optimal combinations of analysis tools focusing on different scales or processes. The approach allows to combine analyses obtained with different tools as well as focusing on individual scales.

With a synthetic test-case we were able to provide guidelines on which formulations to choose among a series of possible algorithms. In particular, we showed that naming process 1 the process which has the highest signal-to-noise ratio (or largest correlation length when the other process has a similar signal-to-noise ratio), then process 1 can be efficiently analyzed by an iterative method P1a. The other process then is optimally reconstructed with another formula P2b and the combination of the two provides an analysis which is close to the theoretical optimal interpolation even with a reduced number of iterations.

Multiscale optimal interpolation

J.-M. Beckers et al.

Title Page

Abstract

Introduction

Conclusions

References

Tables

Figures

◀

▶

◀

▶

Back

Close

Full Screen / Esc

Printer-friendly Version

Interactive Discussion



Multiscale optimal interpolation

J.-M. Beckers et al.

Title Page

Abstract

Introduction

Conclusions

References

Tables

Figures

◀

▶

◀

▶

Back

Close

Full Screen / Esc

Printer-friendly Version

Interactive Discussion



This was then implemented in a real application where it was shown that with the new approach we can indeed retrieve fine-scale features previously filtered out. The iterative version with a combination of DINEOF-based EOF covariances and local optimal interpolation called DINEOFI behaved best, but an alternative cheaper version is to use the DINEOF analysis itself augmented by the analysis of residuals. But we have shown that the latter, quite natural approach, was suboptimal in all situations.

Further fine-tuning of the real application could be performed but is out of the scope of the present paper, focusing on how to combine two or more analysis tools each one exploiting different covariance specifications. To provide the best possible SST products, the following improvements could be included: we can adopt more complicated expressions of the observational error covariances, exploiting the preliminary outliers detection offered by DINEOF and the quality-flag value of the original data. In this case, suspect pixels (near clouds or with statistically too large residuals) can be flagged and see their observational error increased. This should lead to further improvement in the noise filtering. The temporal covariance functions used in the local optimal interpolation could be modulated by a cosine function to take into account the 12 h cycle identified in the residuals and provide better estimates for clouds present during several hours.

Appendix A

Proof of scale-selective analysis formula

With two processes, if we want to isolate the best analysis for process 1, it can be obtained with the gain matrix Eq. (2) in the presence of two scales:

$$\bar{\mathbf{K}}_1 = \mathbf{B}_1 \mathbf{H}^T \left(\mathbf{H} \mathbf{B}_1 \mathbf{H}^T + \mathbf{H} \mathbf{B}_2 \mathbf{H}^T + \mathbf{R} \right)^{-1} \quad (\text{A1})$$

We will now prove Eq. (6) rewritten as

$$\mathbf{B}_1 \mathbf{H}^T \left(\mathbf{H} \mathbf{B}_1 \mathbf{H}^T + \mathbf{H} \mathbf{B}_2 \mathbf{H}^T + \mathbf{R} \right)^{-1} = \mathbf{G}^{-1} \mathbf{K}_1 (\mathbf{I} - \mathbf{H} \mathbf{K}_2) \quad (\text{A2})$$

with $\mathbf{G} = \mathbf{I} - \mathbf{K}_1 \mathbf{H} \mathbf{K}_2 \mathbf{H}$ supposed to be invertible and \mathbf{K}_1 and \mathbf{K}_2 defined by Eq. (3).

5 Multiplying each side to the left by \mathbf{G} and to the right by $\left(\mathbf{H} \mathbf{B}_1 \mathbf{H}^T + \mathbf{H} \mathbf{B}_2 \mathbf{H}^T + \mathbf{R} \right)$, we need to prove that

$$\mathbf{G} \mathbf{B}_1 \mathbf{H}^T = \mathbf{K}_1 (\mathbf{I} - \mathbf{H} \mathbf{K}_2) \left(\mathbf{H} \mathbf{B}_1 \mathbf{H}^T + \mathbf{H} \mathbf{B}_2 \mathbf{H}^T + \mathbf{R} \right) \quad (\text{A3})$$

which, by using the definitions of \mathbf{G} and \mathbf{K}_1 is true if

$$10 \mathbf{I} - \left(\mathbf{H} \mathbf{B}_1 \mathbf{H}^T + \mathbf{R} \right) \mathbf{H} \mathbf{K}_2 \mathbf{H} \mathbf{B}_1 \mathbf{H}^T = \left(\mathbf{H} \mathbf{B}_1 \mathbf{H}^T + \mathbf{R} \right)^{-1} (\mathbf{I} - \mathbf{H} \mathbf{K}_2) \left(\mathbf{H} \mathbf{B}_1 \mathbf{H}^T + \mathbf{H} \mathbf{B}_2 \mathbf{H}^T + \mathbf{R} \right) \quad (\text{A4})$$

which, multiplying each side by $\left(\mathbf{H} \mathbf{B}_1 \mathbf{H}^T + \mathbf{R} \right)$ is true if

$$\mathbf{H} \mathbf{B}_1 \mathbf{H}^T + \mathbf{R} - \mathbf{H} \mathbf{K}_2 \mathbf{H} \mathbf{B}_1 \mathbf{H}^T = (\mathbf{I} - \mathbf{H} \mathbf{K}_2) \left(\mathbf{H} \mathbf{B}_1 \mathbf{H}^T + \mathbf{H} \mathbf{B}_2 \mathbf{H}^T + \mathbf{R} \right) \quad (\text{A5})$$

15 which is true if

$$-\mathbf{H} \mathbf{K}_2 \mathbf{H} \mathbf{B}_1 \mathbf{H}^T = \mathbf{H} \mathbf{B}_2 \mathbf{H}^T - \mathbf{H} \mathbf{K}_2 \left(\mathbf{H} \mathbf{B}_1 \mathbf{H}^T + \mathbf{H} \mathbf{B}_2 \mathbf{H}^T + \mathbf{R} \right) \quad (\text{A6})$$

which in turn is true if

$$20 0 = \mathbf{H} \mathbf{B}_2 \mathbf{H}^T - \mathbf{H} \mathbf{K}_2 \left(\mathbf{H} \mathbf{B}_2 \mathbf{H}^T + \mathbf{R} \right) \quad (\text{A7})$$

Since the latter is true by virtue of the definition of \mathbf{K}_2 , we proved Eq. (6). Then, using Eq. (B1) we also prove Eq. (7). From there, by interchanging indices 1 and 2 we also prove Eq. (12).

We can also prove that Eqs. (4) and (6) are equivalent. We need to show that with $\mathbf{F} = \mathbf{I} - \mathbf{K}_2 \mathbf{H} \mathbf{K}_1 \mathbf{H}$

$$\mathbf{K}_1 - \mathbf{K}_1 \mathbf{H} \mathbf{F}^{-1} \mathbf{K}_2 (\mathbf{I} - \mathbf{H} \mathbf{K}_1) = \mathbf{G}^{-1} \mathbf{K}_1 (\mathbf{I} - \mathbf{H} \mathbf{K}_2) \quad (\text{A8})$$

5 which is true if

$$\mathbf{G} \mathbf{K}_1 - \mathbf{G} \mathbf{K}_1 \mathbf{H} \mathbf{F}^{-1} \mathbf{K}_2 (\mathbf{I} - \mathbf{H} \mathbf{K}_1) = \mathbf{K}_1 (\mathbf{I} - \mathbf{H} \mathbf{K}_2) \quad (\text{A9})$$

itself true if

$$\mathbf{K}_1 \mathbf{H} \mathbf{K}_2 (\mathbf{I} - \mathbf{H} \mathbf{K}_1) = \mathbf{G} \mathbf{K}_1 \mathbf{H} \mathbf{F}^{-1} \mathbf{K}_2 (\mathbf{I} - \mathbf{H} \mathbf{K}_1) \quad (\text{A10})$$

which is the case if

$$\mathbf{K}_1 \mathbf{H} = \mathbf{G} \mathbf{K}_1 \mathbf{H} \mathbf{F}^{-1} \quad (\text{A11})$$

or if

$$\mathbf{K}_1 \mathbf{H} \mathbf{F} = \mathbf{G} \mathbf{K}_1 \mathbf{H} \quad (\text{A12})$$

which is true. Hence we proved Eq. (4). Then application of Eqs. (B2) to (4) proves Eq. (5). From there, as before, interchanging indices 1 and 2 yields Eq. (11) and all our identities are verified.

20 Appendix B

Useful matrix identity

If the inverse matrices involved in the following expression exist, then the following identity holds for any (size compatible) matrices \mathbf{H} , \mathbf{K}_1 and \mathbf{K}_2

$$(\mathbf{I} - \mathbf{K}_1 \mathbf{H} \mathbf{K}_2 \mathbf{H})^{-1} \mathbf{K}_1 = \mathbf{K}_1 (\mathbf{I} - \mathbf{H} \mathbf{K}_2 \mathbf{H} \mathbf{K}_1)^{-1}. \quad (\text{B1})$$

25

Title Page	
Abstract	Introduction
Conclusions	References
Tables	Figures
◀	▶
◀	▶
Back	Close
Full Screen / Esc	
Printer-friendly Version	
Interactive Discussion	



This can be easily shown by an application of the Woodbury formula or a direct proof obtained by multiplying to the right by $(\mathbf{I} - \mathbf{H}\mathbf{K}_2\mathbf{H}\mathbf{K}_1)$ and to the left by $(\mathbf{I} - \mathbf{K}_1\mathbf{H}\mathbf{K}_2\mathbf{H})$. A similar expression can be obtained by interchanging indices 1 and 2:

$$(\mathbf{I} - \mathbf{K}_2\mathbf{H}\mathbf{K}_1\mathbf{H})^{-1}\mathbf{K}_2 = \mathbf{K}_2(\mathbf{I} - \mathbf{H}\mathbf{K}_1\mathbf{H}\mathbf{K}_2)^{-1}. \quad (\text{B2})$$

Acknowledgements. DINEOF was developed by projects funded by the Belgian Science Policy (BELSPO) in the context of RECOLOUR (SR/00/111), BELCOLOUR-2 (SR/00/104), HiSea (SR/12/140), BESST (SR/12/158) and GEOCOLOR (SR/00/139). All projects were part of the Research Program For Earth Observation “STEREO II”. This research was also supported by the SANGOMA Project (European FP7-SPACE-2011 project, Grant 283580). The F.R.S.-FNRS is acknowledged for providing supercomputing access. This is a MARE publication.

References

- Alvera-Azcárate, A., Barth, A., Rixen, M., and Beckers, J.-M.: Reconstruction of incomplete oceanographic data sets using Empirical Orthogonal Functions. Application to the Adriatic Sea Surface Temperature, *Ocean Model.*, 9, 325–346, doi:10.1016/j.ocemod.2004.08.001, 2005. 896
- Alvera-Azcárate, A., Barth, A., Beckers, J.-M., and Weisberg, R. H.: Multivariate reconstruction of missing data in sea surface temperature, chlorophyll and wind satellite field, *J. Geophys. Res.*, 112, C03008, doi:10.1029/2006JC003660, 2007. 896
- Beckers, J.-M. and Nihoul, J.: Model of the Algerian Current’s instability, *J. Marine Syst.*, 3, 441–451, 1992. 919
- Beckers, J.-M. and Rixen, M.: EOF calculation and data filling from incomplete oceanographic datasets, *J. Atmos. Ocean. Tech.*, 20, 1839–1856, 2003. 896
- Beckers, J.-M., Rixen, M., Brasseur, P., Brankart, J.-M., Elmoussaoui, A., Crépon, M., Herbaut, C., Martel, F., Van den Berghe, F., Mortier, L., Lascaratos, A., Drakopoulos, P., Korres, P., Pinardi, N., Masetti, E., Castellari, S., Carini, P., Tintore, J., Alvarez, A., Monserat, S., Parrilla, D., Vautard, R., and Speich, S.: Model intercomparison in the Mediterranean. The MedMEx simulations of the seasonal cycle, *J. Marine Syst.*, 33–34, 215–251, 2002. 918

Multiscale optimal interpolation

J.-M. Beckers et al.

Title Page

Abstract

Introduction

Conclusions

References

Tables

Figures

◀

▶

◀

▶

Back

Close

Full Screen / Esc

Printer-friendly Version

Interactive Discussion



Multiscale optimal interpolation

J.-M. Beckers et al.

Title Page

Abstract

Introduction

Conclusions

References

Tables

Figures

◀

▶

◀

▶

Back

Close

Full Screen / Esc

Printer-friendly Version

Interactive Discussion



- Beckers, J.-M., Barth, A., and Alvera-Azcárate, A.: DINEOF reconstruction of clouded images including error maps – application to the Sea-Surface Temperature around Corsican Island, *Ocean Sci.*, 2, 183–199, doi:10.5194/os-2-183-2006, 2006. 899, 909
- Bracewell, R.: *The Fourier Transform and its Applications*, 2nd Edn., rev., international student ed Edn., McGraw-Hill, New York, 1986. 916
- Brasseur, P., Beckers, J.-M., Brankart, J.-M., and Schoenauen, R.: Seasonal temperature and salinity fields in the Mediterranean Sea: climatological analyses of a historical data set, *Deep-Sea Res. Pt. I*, 43, 159–192, doi:10.1016/0967-0637(96)00012-X, 1996. 898
- Bretherton, F. P., Davis, R. E., and Fandry, C.: A technique for objective analysis and design of oceanographic instruments applied to MODE-73, *Deep-Sea Res.*, 23, 559–582, doi:10.1016/0011-7471(76)90001-2, 1976. 896
- Brisson, A., Le Borgne, P., and Marsouin, A.: Results of one year of preoperational production of sea surface temperatures from GOES-8, *J. Atmos. Ocean. Tech.*, 19, 1638–1652, 2002. 914, 917
- Cushman-Roisin, B. and Beckers, J.-M.: *Introduction to Geophysical Fluid Dynamics, Physical and Numerical Aspects*, Academic Press, 2011. 898, 902
- Daley, R.: *Atmospheric Data Analysis*, Vol. 2, Cambridge University Press, 1993. 900
- Delhomme, J.: Kriging in the hydrosociences, *Adv. Water Resour.*, 1, 251–266, doi:10.1016/0309-1708(78)90039-8, 1978. 896
- Donlon, C. J., Martin, M., Stark, J., Roberts-Jones, J., Fiedler, E., and Wimmer, W.: The operational sea surface temperature and sea ice analysis (OSTIA) system, *Remote Sens. Environ.*, 116, 140–158, 2012. 896
- Eastwood, S., Le Borgne, P., Péré, S., and Poulter, D.: Diurnal variability in sea surface temperature in the Arctic, *Remote Sens. Environ.*, 115, 2594–2602, 2011. 912
- EUMETSAT: *Geostationary sea surface temperature product user manual*, available at: <http://www.osi-saf.org> (last access: 18 March 2014), 2011. 912
- Fisher, M.: Background error covariance modelling, in: *Seminar on Recent Development in Data Assimilation for Atmosphere and Ocean*, 45–63, 2003. 898
- Gandin, L. S.: *Objective Analysis of Meteorological Fields*, Tech. rep., Israel Program for Scientific Translations, Jerusalem, 1965. 896
- Ganzedo, U., Alvera-Azcárate, A., Esnaola, G., Ezcurra, A., and Saenz, J.: Reconstruction of sea surface temperature by means of DINEOF: a case study during the fishing season in the

Multiscale optimal interpolation

J.-M. Beckers et al.

Title Page

Abstract

Introduction

Conclusions

References

Tables

Figures

◀

▶

◀

▶

Back

Close

Full Screen / Esc

Printer-friendly Version

Interactive Discussion



Bay of Biscay, *Int. J. Remote Sens.*, 32, 933–950, doi:10.1080/01431160903491420, 2011. 896

Golub, G. H. and Van Loan, C. F.: *Matrix Computations*, Vol. 3, JHU Press, 2012. 909

Kalnay, E.: *Atmospheric Modeling, Data Assimilation and Predictability*, 1st Edn., Cambridge University Press, 2002. 898

Kaplan, A., Kushnir, Y., and Cane, M. A.: Reduced space optimal interpolation of historical marine sea level pressure: 1854–1992, *J. Climate*, 13, 2987–3002, doi:10.1175/1520-0442(2000)013<2987:RSOIOH>2.0.CO;2, 2000. 899

Karagali, I., Høyer, J., and Hasager, C.: SST diurnal variability in the North Sea and the Baltic Sea, *Remote Sens. Environ.*, 121, 159–170, 2012. 912

Kawai, Y., Kawamura, H., Takahashi, S., Hosoda, K., Murakami, H., Kachi, M., and Guan, L.: Satellite-based high-resolution global optimum interpolation sea surface temperature data, *J. Geophys. Res.-Oceans*, 111, C06016, doi:10.1029/2005JC003313, 2006. 896

Le Borgne, P., Roquet, H., and Merchant, C.: Estimation of sea surface temperature from the Spinning Enhanced Visible and Infrared Imager, improved using numerical weather prediction, *Remote Sens. Environ.*, 115, 55–65, 2011. 912

Le Borgne, P., Legendre, G., and Péré, S.: Comparison of MSG/SEVIRI and drifting buoy derived diurnal warming estimates, *Remote Sens. Environ.*, 124, 622–626, 2012. 912

Marullo, S., Santoleri, R., Banzon, V., Evans, R., and Guarracino, M.: A diurnal-cycle resolving sea surface temperature product for the tropical Atlantic, *J. Geophys. Res.-Oceans*, 115, C05011, doi:10.1029/2009JC005466, 2010. 912

Marullo, S., Santoleri, R., Ciani, D., Borgne, P. L., Péré, S., Pinardi, N., Tonani, M., and Nardone, G.: Combining model and geostationary satellite data to reconstruct hourly SST field over the Mediterranean Sea, *Remote Sens. Environ.*, online first, doi:10.1016/j.rse.2013.11.001, 2013. 912, 914

Millot, C.: Circulation in the Western Mediterranean Sea, *Oceanol. Acta*, 10, 143–149, 1987. 918, 919

Nardelli, B. B., Tronconi, C., Pisano, A., and Santoleri, R.: High and ultra-high resolution processing of satellite sea surface temperature data over Southern European Seas in the framework of MyOcean project, *Remote Sens. Environ.*, 129, 1–16, doi:10.1016/j.rse.2012.10.012, 2013. 896

Nikolaidis, A., Georgiou, G., Hadjimitsis, D., and Akylas, E.: Filling in missing sea-surface temperature satellite data over the Eastern Mediterranean sea using the DINEOF algo-

Multiscale optimal interpolation

J.-M. Beckers et al.

Title Page

Abstract

Introduction

Conclusions

References

Tables

Figures

◀

▶

◀

▶

Back

Close

Full Screen / Esc

Printer-friendly Version

Interactive Discussion



rithm, Central European Journal of Geosciences, online first, doi:10.2478/s13533-012-0148-1, 2013. 896

Parrish, D. and Derber, J.: The National Meteorological Center's spectral statistical interpolation analysis system, *Mon. Weather Rev.*, 120, 1747–1763, 1992. 898

Reynolds, R. W. and Smith, T. M.: Improved global sea surface temperature analyses, *J. Climate*, 7, 929–948, 1994. 896, 899

Sheng, Z., Shi, H.-Q., and Ding, Y.-Z.: Missing satellite-based sea surface temperature data reconstructed by DINEOF method, *Advances in Marine Science*, 2, 017, 2009. 896

Simpson, J.: On the accurate detection and enhancement of oceanic features observed in satellite data, *Remote Sens. Environ.*, 33, 17–33, 1990. 919

Sirjacobs, D., Alvera-Azcárate, A., Barth, A., Park, Y., Nechad, B., Ruddick, K., and Beckers, J.-M.: Cloud filling of total suspended matter, chlorophyll and sea surface temperature remote sensing products by the data interpolation with empirical orthogonal functions methodology, application to the BELCOLOUR-1 database, *ESA Special Publication*, Vol. SP666, available at: <http://orbi.ulg.ac.be/handle/2268/6552> (last access: 18 March 2014), 2008. 897

Stark, J. D., Donlon, C. J., Martin, M. J., and McCulloch, M. E.: OSTIA: an operational, high resolution, real time, global sea surface temperature analysis system, in: *OCEANS 2007 – Europe*, IEEE, 1–4, 2007. 896

Stuart-Menteth, A. C., Robinson, I. S., and Challenor, P. G.: A global study of diurnal warming using satellite-derived sea surface temperature, *J. Geophys. Res.-Oceans*, 108, 3155, doi:10.1029/2002JC001534, 2003. 912

Troupin, C., Machin, F., Ouberdous, M., Sirjacobs, D., Barth, A., and Beckers, J.-M.: High-resolution Climatology of the North-East Atlantic using Data-Interpolating Variational Analysis (DIVA), *J. Geophys. Res.*, 115, C08005, doi:10.1029/2009JC005512, 2010. 903

Volpe, G., Colella, S., Forneris, V., Tronconi, C., and Santoleri, R.: The Mediterranean Ocean Colour Observing System – system development and product validation, *Ocean Sci.*, 8, 869–883, doi:10.5194/os-8-869-2012, 2012. 897

Wackernagel, H.: *Multivariate Geostatistics*, Springer, 2003. 898

Wang, Y. and Liu, D.: Reconstruction of satellite chlorophyll-a data using a modified DINEOF method: a case study in the Bohai and Yellow seas, China, *Int. J. Remote Sens.*, 35, 204–217, doi:10.1080/01431161.2013.866290, 2014. 896

Young, N.: The rate of convergence of a matrix power series, *Linear Algebra Appl.*, 35, 261–278, doi:10.1016/0024-3795(81)90278-0, 1981. 900

Multiscale optimal interpolation

J.-M. Beckers et al.

Table 1. Average error for different analysis formulations of process 1. Column 5 of the upper part shows the same result as column 3, since it can be shown that without iterations, the formulations are equivalent. So column 5 of the upper part of the table is essentially giving confidence that the implementation is correct.

Case	K_1	$K_1(I - HK_2)$	0 it P1a	0 it P1b
1	1.3969	3.2775	1.2212	3.2775
2	1.8056	2.0853	1.6121	2.0853
3	1.1970	1.4024	1.0634	1.4024
4	1.0620	7.4532	1.0215	7.4532
5	1.0055	1.2405	1.0038	1.2405
6	1.9071	2.9159	1.6922	2.9159
7	1.9422	2.1873	1.8183	2.1873
Case	2 it P1a	2 it P1b	20 it P1a	20 it P1b
1	1.0916	2.2260	1.0007	1.0057
2	1.4012	1.8109	1.0281	1.0779
3	1.0205	1.1012	1.0024	1.0024
4	1.0044	2.6406	0.9982	1.0021
5	1.0021	1.1195	0.9997	1.0069
6	1.5009	2.5738	1.0894	1.4318
7	1.6686	2.0194	1.2510	1.3978

Title Page

Abstract Introduction

Conclusions References

Tables Figures

◀ ▶

◀ ▶

Back Close

Full Screen / Esc

Printer-friendly Version

Interactive Discussion



Multiscale optimal interpolation

J.-M. Beckers et al.

Title Page

Abstract

Introduction

Conclusions

References

Tables

Figures

◀

▶

◀

▶

Back

Close

Full Screen / Esc

Printer-friendly Version

Interactive Discussion



Table 3. Average error for different simplified analysis formulations for the overall analysis.

Case	\tilde{K}_{00}	\tilde{K}_{10}	\tilde{K}_{01}	\tilde{K}_{11}
1	6.2802	1.0088	1.0085	5.6440
2	21.6620	1.0165	1.0200	19.8658
3	1.4088	1.0371	1.0357	1.3120
4	4.7596	2.2262	1.0231	6.5037
5	1.5216	1.1202	1.0015	1.3122
6	2.5735	1.2828	1.1630	2.7218
7	19.8920	1.0089	1.0373	19.0295

Multiscale optimal interpolation

J.-M. Beckers et al.

Title Page

Abstract

Introduction

Conclusions

References

Tables

Figures

◀

▶

◀

▶

Back

Close

Full Screen / Esc

Printer-friendly Version

Interactive Discussion



Table 4. Average error for iterative versions for the overall analysis. Zero, two and twenty iterations.

Case	0 it P1a + P2a	0 it P1a + P2b	0 it P1b + P2a	0 it P1b + P2b
1	4.6928	1.0220	1.0385	5.6440
2	18.0134	1.0784	1.0119	19.8658
3	1.1679	1.0071	1.0559	1.3120
4	2.9738	1.0055	2.8756	6.5037
5	1.3133	1.0016	1.0656	1.3122
6	2.3563	1.1118	1.2926	2.7218
7	18.0300	1.0737	1.0139	19.0295
Case	2 it P1a + P2a	2 it P1a + P2b	2 it P1b + P2a	2 it P1b + P2b
1	2.9137	1.0017	1.0203	3.3676
2	13.1811	1.0130	1.0077	14.2558
3	1.0560	1.0014	1.0073	1.0823
4	1.8108	1.0015	1.2031	2.4070
5	1.1680	1.0005	1.0195	1.1583
6	2.0934	1.0696	1.2255	2.3798
7	15.3637	1.0211	1.0113	16.0365
Case	20 it P1a + P2a	20 it P1a + P2b	20 it P1b + P2a	20 it P1b + P2b
1	1.0086	0.9998	0.9999	1.0102
2	2.0564	0.9991	0.9996	2.1293
3	1.0006	1.0006	1.0006	1.0006
4	1.0034	1.0009	1.0010	1.0043
5	1.0101	1.0000	1.0006	1.0094
6	1.3308	1.0056	1.0290	1.3799
7	6.6037	1.0004	1.0024	6.7399

Multiscale optimal interpolation

J.-M. Beckers et al.

Table 5. Skill scores and correlation coefficients for the four SEVIRI setups and the different methods. DINEOF stands for the direct use of standard DINEOF results. DINEOF + \mathbf{K}_2 uses the simple approach of adding a local optimal interpolation of residuals. DINEOF+10 iter stands for the method in which we start from DINEOF results and then apply the iterative version using \mathbf{K}_1 based on the EOFs. Version \mathbf{K}_1 uses only the EOF based covariances, $\tilde{\mathbf{K}}_{01}$ stands for the simple approach when we add the local optimal interpolation of residuals to the previous solution and finally the last two lines correspond to the full method with no iterations or 10 iterations (for inner iterations within \mathbf{K}_1 combining space- and time-EOF based interpolations, iterations are maintained in all cases).

	Setup 1		Setup 2		Setup 3		Setup 4	
	<i>S</i>	<i>r</i>	<i>S</i>	<i>r</i>	<i>S</i>	<i>r</i>	<i>S</i>	<i>r</i>
δ_D	0.496K		0.308K		0.492K		0.285K	
Cloud fraction	42.06%		34.09%		35.29%		27.02%	
<i>N</i> EOF modes	38		37		38		40	
DINEOF	0.00	0.9371	0.00	0.9699	0.00	0.9707	0.00	0.9824
DINEOF + \mathbf{K}_2	0.21	0.9507	0.45	0.9835	0.21	0.9769	0.40	0.9895
DINEOF + 10 it	-1.25	0.8476	-1.79	0.9149	-0.51	0.9559	-0.97	0.9650
\mathbf{K}_1	0.24	0.9516	0.22	0.9764	0.18	0.9760	0.18	0.9855
$\tilde{\mathbf{K}}_{01}$	0.33	0.9576	0.47	0.9839	0.28	0.9791	0.42	0.9899
DINEOFOI 0 it	0.34	0.9579	0.47	0.9840	0.29	0.9792	0.43	0.9899
DINEOFOI 10 it	0.37	0.9602	0.49	0.9845	0.31	0.9798	0.44	0.9901

[Title Page](#)
[Abstract](#)
[Introduction](#)
[Conclusions](#)
[References](#)
[Tables](#)
[Figures](#)
[◀](#)
[▶](#)
[◀](#)
[▶](#)
[Back](#)
[Close](#)
[Full Screen / Esc](#)
[Printer-friendly Version](#)
[Interactive Discussion](#)


Multiscale optimal interpolation

J.-M. Beckers et al.

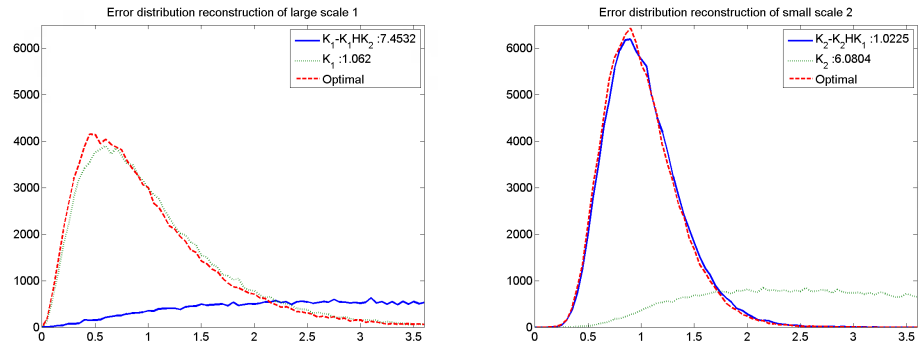


Fig. 1. Histogram of scaled errors for reconstruction of process 1 (left) and process 2 (right). We see that for process 1 it is better to use the full data set, whereas for process 2 it is better to work with residuals, i.e. data from which we subtract the analysis of the process 1.

Title Page

Abstract Introduction

Conclusions References

Tables Figures

◀ ▶

◀ ▶

Back Close

Full Screen / Esc

Printer-friendly Version

Interactive Discussion



Multiscale optimal interpolation

J.-M. Beckers et al.

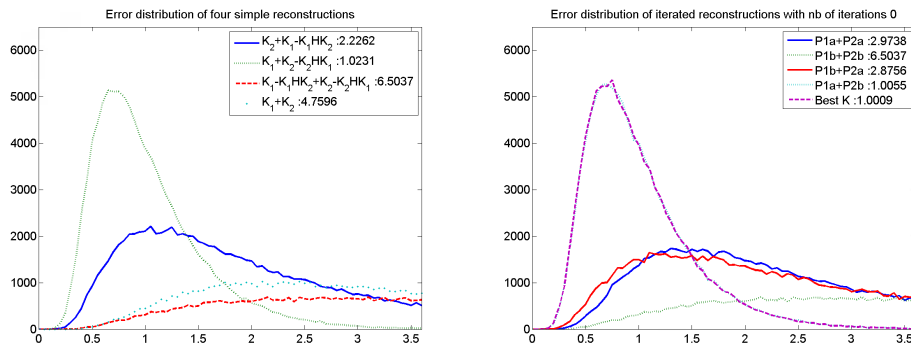


Fig. 2. Histogram of scaled errors for simple reconstructions of the total field (left) and with zero iterations in the new formulations. For reference the distribution of the optimal solution is also shown, proving that not only the average error of the new method combining P1a and P2b is optimal, but also the error distribution falls onto the optimal one.

Title Page

Abstract

Introduction

Conclusions

References

Tables

Figures

◀

▶

◀

▶

Back

Close

Full Screen / Esc

Printer-friendly Version

Interactive Discussion



Multiscale optimal interpolation

J.-M. Beckers et al.

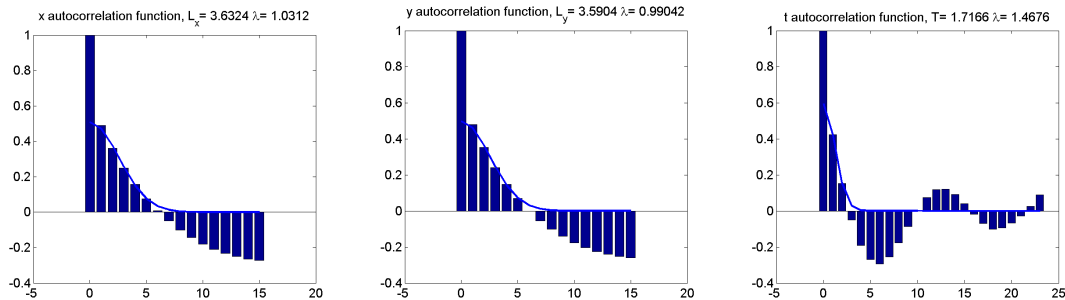


Fig. 4. Spectrum analysis leading to autocorrelation functions, for longitude, latitude and time (from left to right). Autocorrelation is given as a function of distance expressed in number of grid points or time-delay expressed in number of timesteps (hours). The continuous line corresponds to the fitted Gaussian correlation function.

[Title Page](#)[Abstract](#)[Introduction](#)[Conclusions](#)[References](#)[Tables](#)[Figures](#)[◀](#)[▶](#)[◀](#)[▶](#)[Back](#)[Close](#)[Full Screen / Esc](#)[Printer-friendly Version](#)[Interactive Discussion](#)

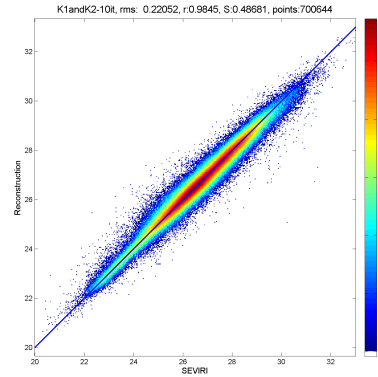
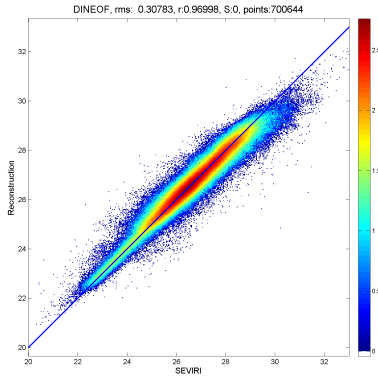
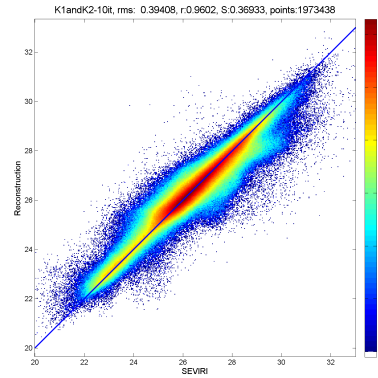
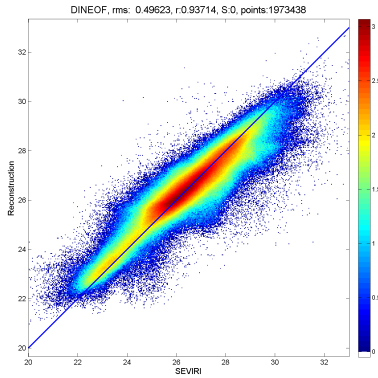


Fig. 5. Correlation at cross-validation points using DINEOF alone and the new method DINE-OFOI in Setup 1 (top) and Setup 2 (below).

Multiscale optimal interpolation

J.-M. Beckers et al.

Title Page

Abstract Introduction

Conclusions References

Tables Figures

◀ ▶

◀ ▶

Back Close

Full Screen / Esc

Printer-friendly Version

Interactive Discussion



Multiscale optimal interpolation

J.-M. Beckers et al.

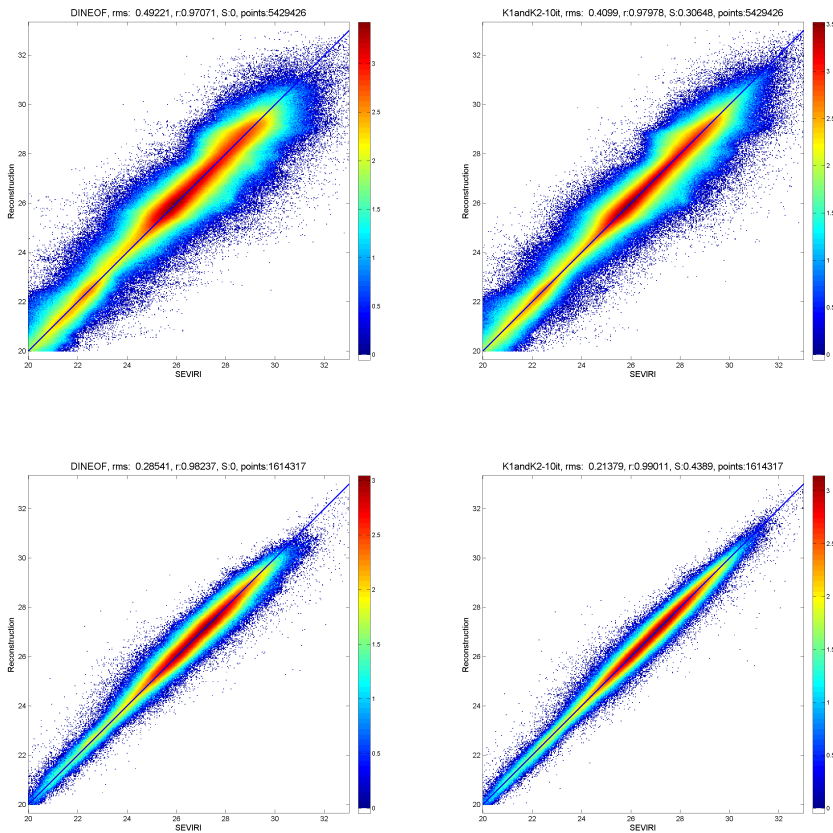


Fig. 6. Correlation at cross-validation points using DINEOF alone and the new method DINE-OFOI in Setup 3 and Setup 4.

Title Page

Abstract Introduction

Conclusions References

Tables Figures

◀ ▶

◀ ▶

Back Close

Full Screen / Esc

Printer-friendly Version

Interactive Discussion



Multiscale optimal interpolation

J.-M. Beckers et al.

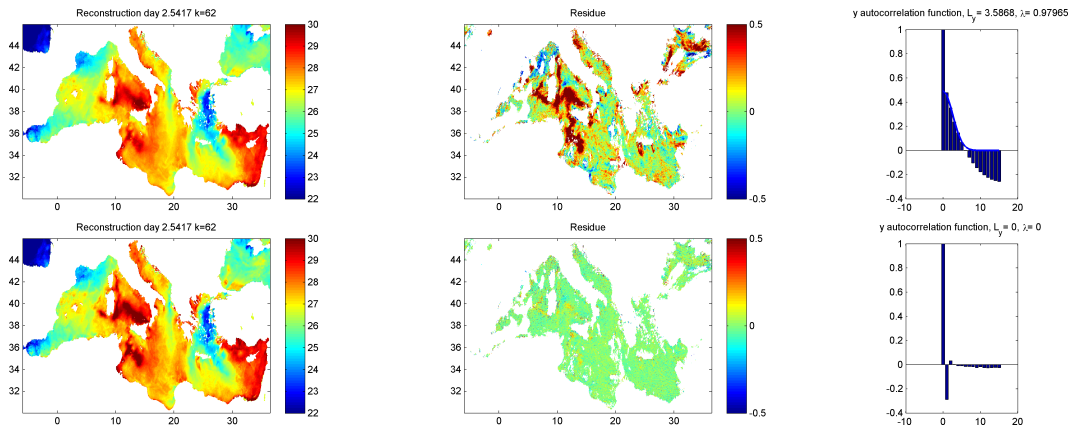


Fig. 7. DINEOF reconstruction, residual and autocorrelation of residuals. DINEOF (top) and new method DINEOFI (lower images).

Title Page

Abstract	Introduction
Conclusions	References
Tables	Figures
◀	▶
◀	▶
Back	Close
Full Screen / Esc	
Printer-friendly Version	
Interactive Discussion	



Multiscale optimal interpolation

J.-M. Beckers et al.

Title Page

Abstract

Introduction

Conclusions

References

Tables

Figures

◀

▶

◀

▶

Back

Close

Full Screen / Esc

Printer-friendly Version

Interactive Discussion

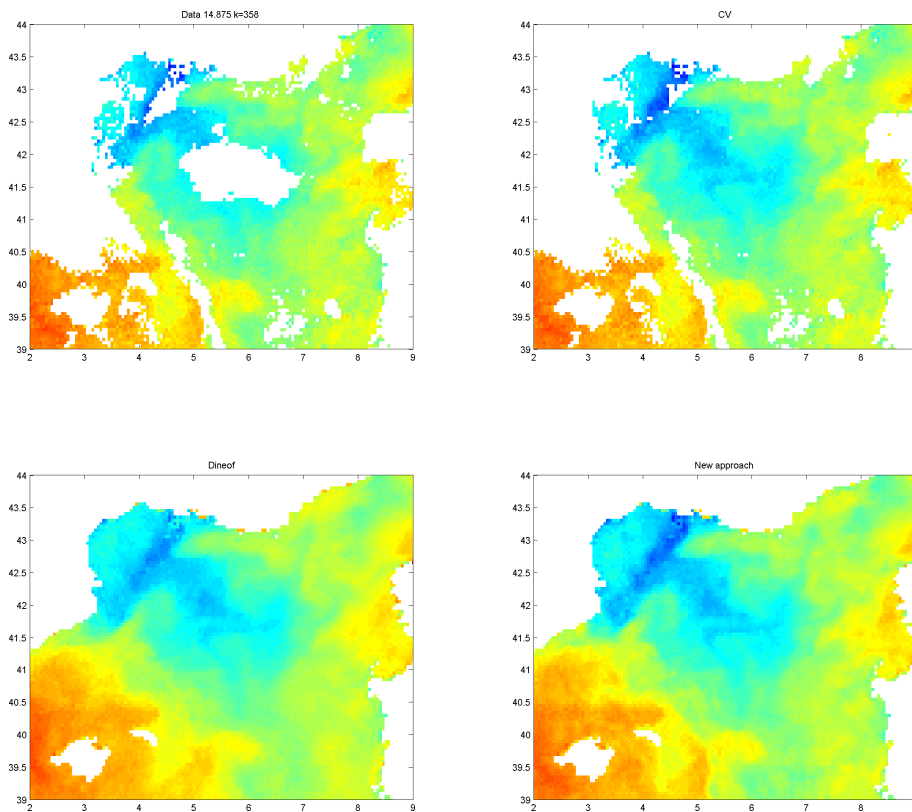


Fig. 8. Data used (upper left panel), data including cross validation data (upper right), DINEOF reconstruction (lower left) and new approach DINEOFOI with 10 iterations (lower right).

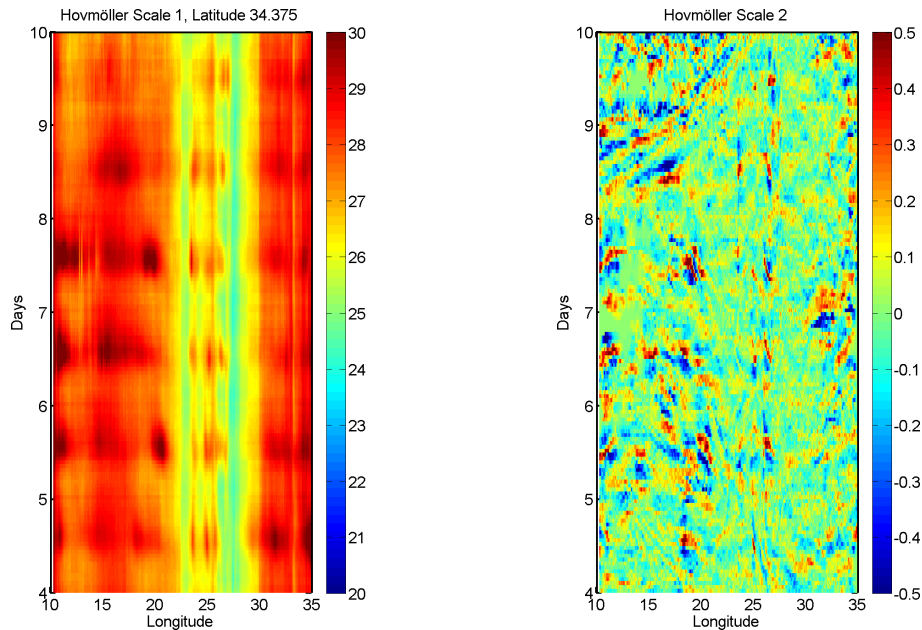


Fig. 9. Hovmöller diagram in the Eastern Mediterranean at latitude 34.375 °N. Temperature as a function of longitude (in degrees) and time (in days) for process 1 (left panel) and process (2) (right panel).

Multiscale optimal interpolation

J.-M. Beckers et al.

Title Page

Abstract Introduction

Conclusions References

Tables Figures

◀ ▶

◀ ▶

Back Close

Full Screen / Esc

Printer-friendly Version

Interactive Discussion



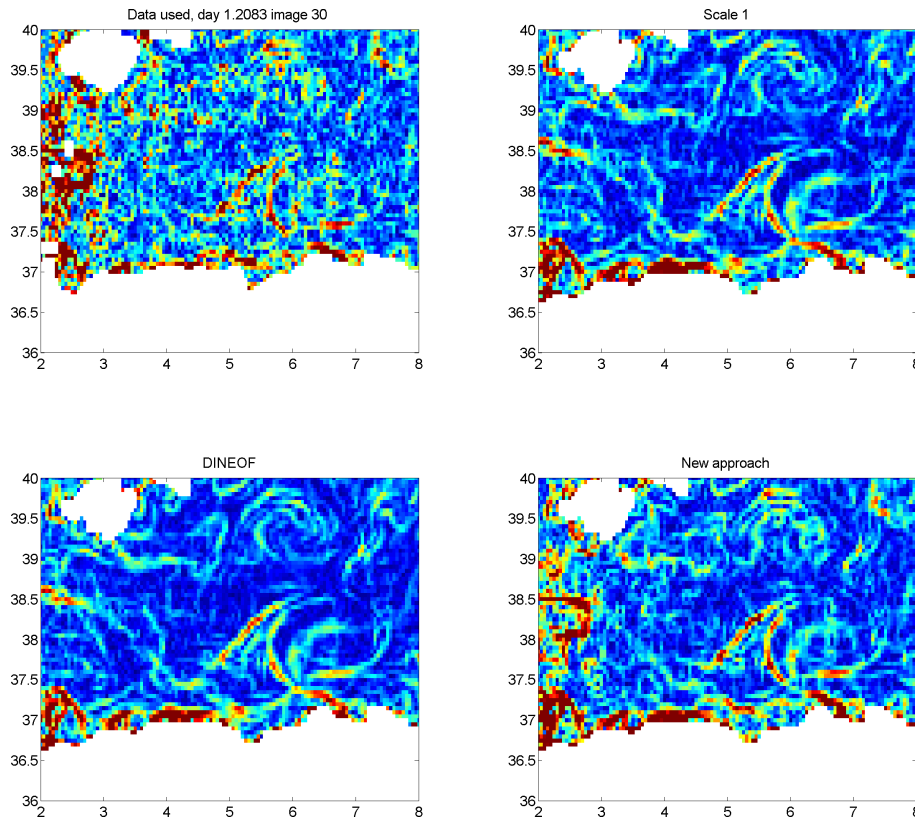


Fig. 10. Sobel-type edge gradient detector applied to raw data (upper left panel), DINEOF (lower left panel), Scale 1 solution with the new method (upper right panel) and new method including both scales (lower right panel). Focus on the African coast in the Western Mediterranean.

Multiscale optimal interpolation

J.-M. Beckers et al.

Title Page

Abstract Introduction

Conclusions References

Tables Figures

◀ ▶

◀ ▶

Back Close

Full Screen / Esc

Printer-friendly Version

Interactive Discussion

